Nanoscale Advances

ROYAL SOCIETY OF CHEMISTRY

COMMUNICATION

View Article Online
View Journal | View Issue

Open Access Article. Published on 15 December 2020. Downloaded on 2/15/2026 2:38:43 PM.
This article is licensed under a Creative Commons Attribution-NonCommercial 3.0 Unported Licence.

Check for updates

Cite this: *Nanoscale Adv.*, 2021, 3, 339

Received 22nd October 2020
Accepted 26th November 2020

DOI: 10.1039/d0na00888e

rsc.li/nanoscale-advances

Fabrication of polyethylene terephthalate (PET) nanoparticles with fluorescent tracers for studies in mammalian cells†

Leah M. Johnson, *[a] Jeffrey B. Mecham,[a] Sai Archana Krovi,[a] Maria M. Moreno Caffaro,[a] Shyam Aravamudhan,[b] Alexander L. Kovach,[a] Timothy R. Fennell[a] and Ninell P. Mortensen[a]

Fluorescent nanoparticles (NPs) comprising polyethylene terephthalate (PET) with a hydrodynamic diameter of 158 ± 2 nm were synthesized in a bottom-up approach. Concentration-dependent uptake and cytotoxicity of PET NPs in macrophages are shown. The fabrication of well-characterized NPs, derived from high-commodity polymers, will support future studies to assess effects on biological systems.

Introduction

Plastics are globally ubiquitous and have supported advancements in society by improving the performance of food and beverage packaging, building materials, healthcare and personal care products, and transportation vehicles.[1] Despite these benefits, there exists an emerging concern involving the fate of plastic debris in the environment.[2–7] An estimated 4900 million metric tons (Mt) of discarded plastics currently reside in landfills or the environment, with the most abundant non-fiber resins including polystyrene (PS), polyethylene (PE), polyvinyl chloride (PVC), polyurethane (PU), polypropylene (PP), and polyethylene terephthalate (PET).[8] In particular, the PET thermoplastic is a semicrystalline, lightweight, and water resistant material[9] that critically serves global markets for packaging, films, and textiles with the worldwide production of the PET resin reaching over 30 million tons in recent years.[10] While recycling tactics exist for PET,[11,12] many PET products are intended for swift disposal and consequently accumulate in the environment, where the material is susceptible to degradation through photochemical, thermal, and mechanical mechanisms.[13–18] Degradation processes could generate randomized fragments of PET contaminants with wide size distributions and morphologies.

Numerous reports highlight the presence of fragmented plastics, termed 'microplastics', in drinking water[19–21] and beverages,[22,23] food,[24–27] and the natural environment.[28] Environmental microplastics can originate from two key sources: intentionally formulated products (*e.g.*, microbead scrubs, toothpaste, cleaners) and plastic debris that physically or chemically degrades after environmental exposures (*e.g.*, UV irradiation, heat, mechanical stress, humidity).[29–32] Because decomposition processes can produce fragments of diverse size, morphology, and composition, efforts are underway to standardize definitions and harmonize scientific communication.[33] This classification of microplastics could ultimately encompass many physicochemical properties,[33,34] but thus far plastic fragments are typically categorized by size. One highly recognized definition by the National Oceanic and Atmospheric Administration (NOAA) refers to microplastic as fragments with diameters <5 mm.[35] Because the size of particles is interrelated to physicochemical properties, a refinement to size classifications will support the full understanding of the fate and behavior of these plastic fragments. For example, recent reports indicate the potential of nano-scale plastics in the environment.[36] Nanomaterials can penetrate biological membranes and be taken up by cells and accumulate within tissues, as evident from the wealth of nanotoxicity studies with various metal NPs.[37–41] Moreover, the high surface area of nanomaterials can serve as carriers of various environmental constituents due to the absorption to the surface of the materials. The ultimate consequence of plastic fragments, together with chemicals absorbed to these plastic vectors,[42] on biological systems remains unknown.

Despite the growing concern over plastic NPs as widespread environmental contaminants, very few studies have investigated the biological effects of nanomaterials that comprise high-volume commodity plastics (*e.g.*, PET, PP, PVC, PU). To date, the majority of reports have focused on the biological responses to commercially available fluorescently-labeled PS NPs.[43,44] One

[a]RTI International 3040 East Cornwallis Drive, Research Triangle Park, NC 27709, USA. E-mail: leahjohnson@rti.org

[b]Joint School of Nanoscience and Nanoengineering, North Carolina A&T State University, 2907 East Gate City Blvd, Greensboro, NC 27401, USA

† Electronic supplementary information (ESI) available. See DOI: 10.1039/d0na00888e

© 2021 The Author(s). Published by the Royal Society of Chemistry

Open Access Article. Published on 15 December 2020. Downloaded on 2/15/2026 2:38:43 PM.
This article is licensed under a Creative Commons Attribution-NonCommercial 3.0 Unported Licence.

key hurdle that hinders further testing of other commodity-based nanoplastics involves the limited availability of highly characterized and biological traceable nanomaterials. In the case of PET, for example, very few reports currently exist that describe the fabrication of PET NPs suited for biological studies. The fabrication of PET NPs has occurred *via* laser ablation[45] and catalytic emulsion polymerization,[46] however, these approaches do not incorporate tracers into the NPs to monitor spatial distribution in cells or small organisms. One encouraging study from Rodríguez-Hernández *et al.* recently reported the synthesis of fluorescently labeled PET NPs for studies in macrophages, but their results also showed aggregation of the NPs.[47]

Herein, we report the synthesis of disperse PET NPs with a tight size distribution using a facile, bottom-up fabrication approach. We further show the incorporation of fluorescent tracers into the NPs that enables visualization and characterization of these PET NPs within mammalian cells.

Materials and methods

Fabrication of PET NPs

A solution of PET was prepared by mixing 0.58 g PET fiber (IZO Home Goods) with 35 mL hexafluoroisopropanol (HFIP) (Sigma-Aldrich, St. Louis, MO, USA) in a 40 mL scintillation vial equipped with a magnetic stir bar that was coated with polytetrafluoroethylene (PTFE). PET solution (10 mL) was added dropwise at 1 mL min^{-1} using a syringe pump (Model # NE-300, New Era Pump Systems, Inc., Farmingdale, NY, USA) with a Poulten & Graf GmbH Fortuna® Optima® 10 mL glass syringe into ultrapure deionized water (75 mL, 18.2 MΩ cm resistivity) at room temperature, resulting in precipitation of PET NPs. The entire contents of the precipitation vessel were transferred to a 250 mL round-bottomed flask and rotary evaporated under vacuum at 55 °C to remove residual HFIP. Upon reduction of the volume in the round-bottomed flask (~30 mL), ultrapure deionized water (~75 mL) was added, and the flask was subjected to rotary evaporation for a second time. The concentrated suspension of particles was pipetted into a 20 mL scintillation vial. Particles containing rhodamine B (Sigma-Aldrich, St. Louis, MO, USA) were formulated using a similar approach as specified above. The tracer solution in HFIP (0.05 mg mL^{-1}) was prepared from a stock solution of 1 mg mL^{-1}. An aliquot of the 0.05 mg mL^{-1} tracer solution (1 mL) was then added to the PET solution prior to precipitation into ultrapure deionized water.

Purification of PET NPs

To remove residual HFIP, the suspension of particles was centrifuged and resuspended. Each wash step consisted of centrifuging the suspension at 13 100 rpm for 5 minutes at room temperature, removing the supernatant, and resuspending in an equal volume of 0.5 mg mL^{-1} Bovine Serum Albumin (BSA) (pH 8.2) to maintain the concentration of the particles in suspension. The particles were resuspended by a 30 second vortex step followed by discrete sonication in a cup horn sonicator (Ultrasonic Liquid Processor S-400, Misonic Inc., Farmingdale, NY) delivering a total of 840 J mL^{-1}. For the first wash step, the initial particle suspension was spiked with BSA to a final concentration of 0.5 mg mL^{-1} before the first centrifugation step. The particles were washed three times and resuspended in a final solution of 0.5 mg mL^{-1} BSA (pH 8.2).

Characterization of PET NPs

Dynamic light scattering (DLS) and zeta potential. The hydrodynamic diameter of the NPs was measured by DLS using the Malvern zetasizer Nano-ZS (Malvern Panalytical, Westborough, MA). The zeta potential was measured using the same instrument with disposable folded capillary zeta cells (Malvern Panalytical, Westborough, MA). For these measurements, NPs were suspended in 0.5 mg mL^{-1} BSA (pH 8.2).

Concentration of NPs and fluorescent tracer. To determine the concentration of particles, an aliquot (1 mL) of PET particles was transferred to a tared 2 mL Eppendorf tube and placed in a vacuum oven under ambient conditions overnight. The tube was weighed the next day to determine the dry particle weight. To determine the concentration of rhodamine B within the particles, dried particles were subsequently dissolved in HFIP (1 mL) and their fluorescence was determined using Synergy MX multi-mode plate reader (BioTek Instruments, Inc, Winooski, VT, USA). The average quantity of rhodamine B loaded into the PET NPs was calculated from two batches and averaged 0.35 mass%. A calibration curve of rhodamine B in HFIP, was obtained *via* serial dilutions of the fluorophore (1.25 μg mL^{-1} stock solution, $\lambda_{ex} = 550$ nm, $\lambda_{em} = 580$ nm).

Fourier-transform infrared spectroscopy (FT-IR). The dried samples were analyzed with a Nicolet 6700 FTIR with a Smart Orbit™ single bounce diamond crystal ATR accessory. The instrument has a deuterated triglycine sulfate (DTGS) detector and a potassium bromide (KBr) beam splitter. Method parameters were set at resolution of 4 and 32 scans, scanning the region 4000–400 cm^{-1}. A background was run on the cleaned crystal before each sample. After the background acquisition was complete, a small amount of sample was added to the diamond crystal, pressure was applied, then data was acquired. The suspension of particles that were used for FT-IR were washed using water instead of 0.5 mg mL^{-1} BSA.

^{19}F nuclear magnetic resonance spectroscopy (^{19}F-NMR). The presence of residual HFIP within the PET NPs was determined by ^{19}F-NMR. The fluorine NMR experiments were performed on a Varian Unity Inova 500 mHz NMR (Palo Alto, CA) with a Nalorac Cryogenics Corporation dedicated H–F observed probe (Martinez, CA). ^{19}F-NMR samples were mixed with D_2O at 10 percent. Total recycling time was 8 seconds. An external reference standard was used to calibrate and quantitate the remaining fluorine using Agilent VnmrJ ver. 4.2 software (Santa Clara, CA) with a limit of detection of 0.02 mM.

Transmission electron microscopy (TEM). PET NPs were prepared using the drop mount method for liquid deposition. PET NPs were pipetted onto 200 mesh carbon coated copper transmission electron microscopy (TEM) grids. The liquid suspension was dried in air on the copper grids inside a HEPA filtered fume hood. Two TEM grids were prepared per sample.

 © 2021 The Author(s). Published by the Royal Society of Chemistry

Open Access Article. Published on 15 December 2020. Downloaded on 2/15/2026 2:38:43 PM. This article is licensed under a Creative Commons Attribution-NonCommercial 3.0 Unported Licence.

The grids were analyzed using a Hitachi H-7000 transmission electron microscope. Multiple images were taken of each sample using an AMT digital camera. Analytical magnifications ranged between 40 000× to 300 000×.

Scanning electron microscopy (SEM). SEM was performed using a Zeiss Auriga field emission scanning electron microscope (FESEM) (Carl Zeiss Microscopy, White Plains, NY) at 5 kV accelerating voltage and a beam current of 10 μA. Prior to SEM analysis, all samples were sputter coated with 6 nm of gold palladium using a low vacuum sputter coater (Leica EM ACE200, Leica Microsystems Inc., Buffalo Grove, IL). The particle diameter was measured using ImageJ (NIH).

Ultraviolet-visible spectroscopy (UV-Vis). Samples were analyzed using a Shimadzu UV-2600 UV-Visible Spectrophotometer (Columbia, MD) with LabSolutions software, version 1.03 (Atlanta, GA) at a wavelength range of 200 to 800 nm. Samples were diluted 1 : 10 and 1 : 100 in BSA, and BSA was used as the blank. A slit width of 2 nm was used with a data interval of 0.5 nm.

Studies in mammalian cells

Endotoxin assay. A pyrochrome test kit with glucashield reconstitution buffer and control standard endotoxin (Associates of Cape Cod Inc, East Falmouth, MA) was used to detect and quantify endotoxins following the manufacturer's protocol. PET-NP and PET-RB NP were diluted to a concentration of 0.2 mg mL^{-1} and 0.3 mg mL^{-1}, respectively, in endotoxin-free limulus amebocyte lysate (LAL) reagent water (Associates of Cape Cod Inc, East Falmouth, MA). Supernatant from PET-NP and PET-RB NP was tested in LAL reagent water. The BSA solution used for washing and suspension of the particles was also tested. To ensure that the PET NPs did not interfere with the assay, positive product controls (PPC) containing a final concentration of 0.5 endotoxin units (EU) per mL were tested in parallel at the same concentration. No interference between the two PET NPs and the assay was detected for the tested concentrations.

Cell culture. PET NP and PET-RB NP toxicity was tested on mouse alveolar macrophage cells, RAW 264.7 (ATCC® TIB-71™, ATCC, Manassas, VA). RAW 264.7 cells were cultured in Dulbecco's modified eagle's medium (Gibco, Life Technologies, Grand Island, NY), supplemented with 10% fetal bovine serum (FBS) (Gibco, Life Technologies, Grand Island, NY) and 100 U penicillin/streptomycin (P/S) (Gibco, Life Technologies, Grand Island, NY). Cells were maintained at 37 °C in 5% humidified CO_2, at a concentration of 1×10^4 cell per mL and passaged twice a week by washing with pre-warmed phosphate-buffered saline (PBS) (Gibco, Life Technologies, Grand Island, NY). RAW 264.7 cells were used between passage numbers 41–45.

Cytotoxicity assays. RAW264.7 were seeded out in a 96 well plate at a concentration of 1×10^5 cells per mL and incubated for 24 hours. NPs suspended in fresh media were added to the cells in a two-fold dilution with concentrations between 0.0005–0.5 mg mL^{-1}. After 24 hours of NP exposure, the media was collected for lactate dehydrogenase (LDH) release measurements. LDH assay (TOX7, Sigma-Aldrich, St. Louis, MO) was done according to the manufacturer protocol to measure the level of LDH released to the media. Briefly, 75 μL of media was analyzed to assess cell viability as a function of cell membrane integrity. Following media collection for LDH measurements, the monolayer was washed with PBS and MTS assay was used to determine viability and metabolic activity in the cells. MTS [3-(4,5-dimethylthiazol-2-yl)-5-(3-carboxymethoxyphenyl)-2-(4-sulfophenyl)-2*H*-tetrazolium] assays (CellTiter 96® AQueous One Solution Cell Proliferation Assay, Promega, Madison, WI) were performed according to the manufacturer protocol. Briefly, the cell reagent solution was added to the cells, and metabolic activity determined by colorimetric measurement of MTS which is reduced to colored formazan by viable, metabolically-active cells. Data are expressed as percentage of their representative controls. All studies were conducted in biological duplicates and at least experimental triplicates. An LDH assay was performed without cells to evaluate any interferences between NPs and the assay, an approximately 50% increase in the background value was observed for 0.5 mg mL^{-1} for both PET-NP and PET-RB NP (ESI 1†). The absorbance of the dose concentrations was measured in the wavelength for MTS assay (490 nm) and showed a concentration dependent increase in the background values, with a five-fold increase in absorbance for the highest concentration, which could mask the MTS response at the high dosing concentration.

Fluorescence microscopy. Cells were seeded at a concentration of 1×10^5 cells per mL in glass bottom Petri dishes (MatTek, Ashland, MA) and after 24 h were exposed to PET-RB NP for 16 h at concentrations of 0.005, 0.05, and 0.5 mg mL^{-1}. Simultaneously with PET-RB NP exposure, CellLight Lysosomes-GFP *BacMam 2.0* (Life Technologies, Grand Island, NY) were added to the cells to stain lysosomes at a count of 25 particles per cell. Cells were subsequentially fixed with 3% paraformaldehyde and 0.1% glutaraldehyde for 30 minutes at room temperature. After three washes with PBS, the cells were stained with 1 : 200 DAPI (Life Technologies, Grand Island, NY) for 15 min at room temperature. Cells were washed three times in PBS before bright field and fluorescence imaging with a 40× objective. Imaging was conducted using an Olympus IX71 inverted microscope with a CCD Microscopy Camera (INFINITY3-3URF, 3.0 Megapixel, CoolLED). Image processing was performed using ImageJ (NIH).

Data analysis. Data are expressed as mean ± standard deviation using the software Prism (GraphPad 7.4, GraphPad Software, San Diego, CA). Test for equality of variances was performed prior to statistical analysis. An unpaired, two-tailed *t*-test (equal variance) or a *t*-test with Welch correction (unequal variance) were used for statistical analysis between doing groups. Statistical significance was at $P < 0.05$.

Results and discussion

Fabrication and characterization of PET NPs

The PET NPs were fabricated with a precipitation method, wherein a solution of PET in HFIP was slowly added to ultrapure water resulting in the formation of NPs. Multiple washing steps were used to remove residual HFIP solvent from the NP

Open Access Article. Published on 15 December 2020. Downloaded on 2/15/2026 2:38:43 PM.
This article is licensed under a Creative Commons Attribution-NonCommercial 3.0 Unported Licence.

formulations, resulting in an undetectable fluorine signal *via* ^{19}F-NMR. While washing the PET NPs with ultrapure water, the particles aggregated and therefore a solution of BSA protein at 0.5 mg mL^{-1} was used instead to maintain particle dispersion during washing steps. Here, utilization of BSA was compatible with subsequent studies in cell culture, as discussed in the following section. However, use of species-specific proteins or alternative surfactants as stabilizing agents of these NPs may be required to align with other biological systems under investigation in future work. To enable detection of the PET NPs within cells, the particles were labeled with rhodamine B (PET-RB) by incorporation of the tracer into the NPs during fabrication.

The spherical morphology of the PET-RB NPs was evident *via* SEM (Fig. 1A) and TEM (Fig. 1B) and no morphological differences were apparent for the PET NPs without tracer (ESI 2†). After washing and resuspending the particles in a BSA solution, the hydrodynamic diameters were 170 ± 3 nm for PET-NPs and 158 ± 2 nm for PET-RB NPs (Fig. 1C and ESI 2†). The washing steps with the BSA solution slightly increased the hydrodynamic diameters, as compared to those of the unwashed samples, but the average size distributions remained below 200 nm with polydispersity indices at 0.2 and 0.1 for PET NP and PET-RB NP, respectively. The average diameters of NPs were also calculated from the SEM images at 95 ± 14 nm for PET NPs and 88 ± 14 nm for PET-RB NPs. The differences between the hydrodynamic diameters and the diameters calculated from SEM images (*i.e.*, dried samples) are expected and could result, in part, from the existence of a BSA corona within in the particle suspensions[48] or from the indirect measurements associated with DLS that relies on fluctuations in the particle scattering intensity in solution.[49] The zeta potential for NPs suspended within the BSA solution was −37 mV for PET NPs and −38 mV for PET-RB NPs, which aligns with the high stability and dispersion of the particles. For example, the PET-RB NPs measured 162 ± 2 nm (polydispersity index of 0.2) after two months of storage at 4 °C.

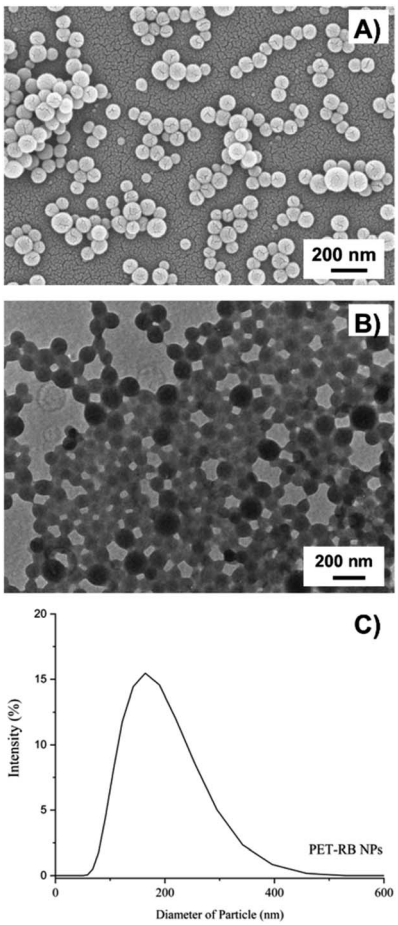

Fig. 1 (A) SEM, (B) TEM, and (C) the DLS curve for PET-RB NPs. The DLS profile is an average of three DLS runs.

To explore the composition of the NPs, FT-IR analysis was performed (Fig. 2). The FT-IR profiles of NPs showed characteristic absorption bands of the PET bulk polymer (ESI 3†),[50–52] including at 1715 cm^{-1} (C=O stretching), 1578 cm^{-1} (stretching of C=C in ring), and 1505 cm^{-1} (in-plane bending of C–H in ring; stretching of C=C in ring), and 1240 cm^{-1} (C=O in-plane bending, C–C stretching, C(=O)–O stretching).[52] As shown in Fig. 2, the prominent IR absorption bands were similar between PET and PET-RB NPs. Interestingly, bands associated with rhodamine B, such as near 1590 cm^{-1} (COO– stretching)[53] were not clearly present for the PET-RB NPs, despite the verification of the fluorescent tracer *via* fluorescence microscopy. The lack of prominent rhodamine B absorbance bands in the FT-IR could be due to the low concentration of the tracer, which was undetectable in the IR spectrum. Additional testing using Raman spectroscopy (ESI 4†), Pyro-GC/MS (ESI 5†), and XPS (ESI 6†) also confirmed various moieties within the PET NPs. These in-depth analyses of the PET NPs support steps towards more standardized NPs for studies in biological systems, as discussed in the next section.

Evaluation of PET NP and PET-RB NP in mammalian cells

Prior to evaluation in mammalian cells, it is critical to ensure the absence of contaminants. To this end, a kinetic turbidity LAL assay was used to ascertain potential endotoxin

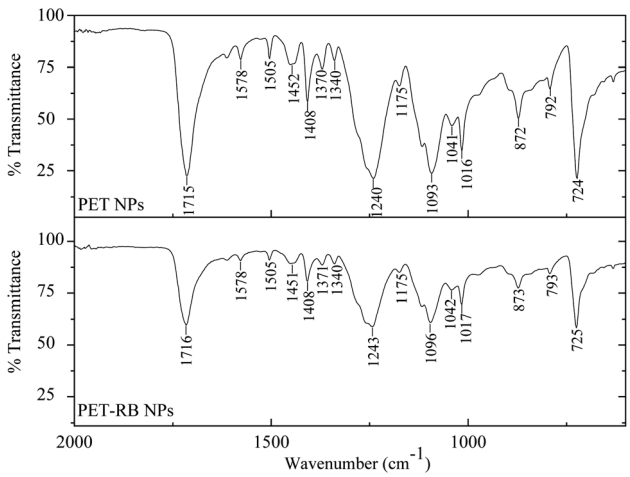

Fig. 2 FT-IR spectra of PET NPs without tracer (top) and with rhodamine B (bottom).

 © 2021 The Author(s). Published by the Royal Society of Chemistry

Open Access Article. Published on 15 December 2020. Downloaded on 2/15/2026 2:38:43 PM.
This article is licensed under a Creative Commons Attribution-NonCommercial 3.0 Unported Licence.

contamination in the NPs. Although levels of endotoxins were detectable, the values were below the recommended FDA limit of 0.5 EU per mL for medical devices[54,55] showing 0.1 EU per mL and 0.064 EU per mL for PET-NPs and PET-RB NPs, respectively. The cytotoxicity and uptake of PET NPs were evaluated in murine alveolar macrophages, RAW264.7 in a dose–response manner. Cytotoxicity was evaluated by determining cell membrane integrity (LDH release) and metabolic activity (MTS) (Fig. 3). A significant increase in LDH release was observed at 0.0625 mg mL^{-1} for PET NP (P-value = 0.0016) and at 0.0010 mg mL^{-1} for PET-RB NP (P-value = 0.0034). We speculate that the PET-RB NP interfered with the cell membrane even at the low concentrations. At a concentration of 0.125 mg mL^{-1} for both PET NPs (160 ± 27.5% of control for PET-NP and 178 ± 18.3% of control for PET-RB NPs) the LDH release continued to scale with increasing concentration, so that LDH release for 0.5 mg mL^{-1} was 506 ± 85% of control for PET NP and 447 ± 46.1% of control for PET-RB NPs. On the other hand, a slight increase in the MTS assay was observed for the lowest concentration of PET NPs. This might be due to an interference between PET NPs and MTS but requires further investigation. Only at the highest tested concentration of PET NPs of 0.5 mg mL^{-1} did the MTS assay show a significant decrease in mitochondrial activity (82.9 ± 8.77% of control for PET-NP and 71.3 ± 29.4% of control for PET-RB NPs). Together these findings suggest that the cell membrane integrity was impacted at a lower NP concentration before mitochondrial activity was altered.

The cellular uptake of PET-RB NPs and resulting morphological changes in RAW264.7 cells were evident from bright field and fluorescence microscopy. Following exposure to a low concentration of 0.005 mg mL^{-1} PET-RB NPs, particles were visible in the cell cytoplasm (Fig. 4D), however at concentrations of 0.05 and 0.5 mg mL^{-1} PET-RB NPs large clusters of NPs were observed intracellularly both in bright field and fluorescence microscopy (Fig. 4, individual fluorescence channels are shown in ESI 7† and overlay of bright field and fluorescence images in ESI 8†). The fluorescence intensity of the larger NP aggregates caused oversaturation at the exposure time needed to visualize individual PET-RB NPs particles, making the aggregates look larger in the fluorescence microscopy images compared to the bright field images. Since the PET-RB NPs showed a low level of

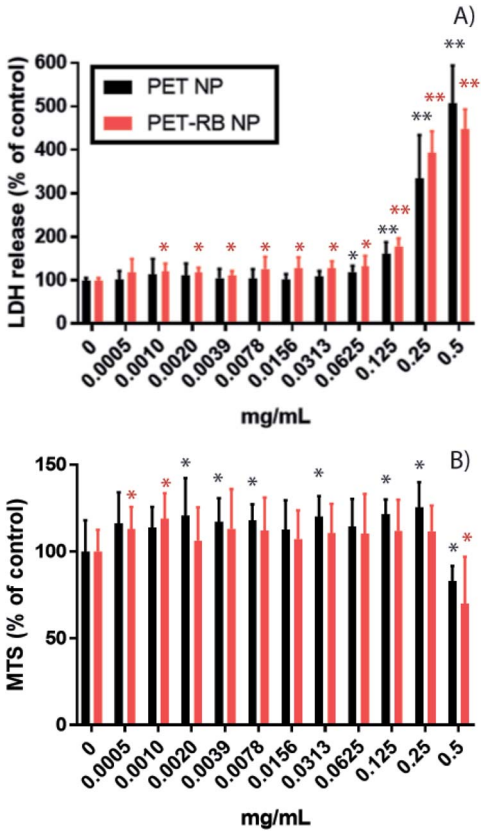

Fig. 3 Cytotoxicity of PET-NP (black bars) and PET-RB NPs (red bars) tested by (A) membrane integrity (LDH release) and (B) metabolic activity (MTS assay). The graphs show mean ± standard deviation. One asterisk indicates P-values <0.05 and two asterisks indicate P-value <0.001.

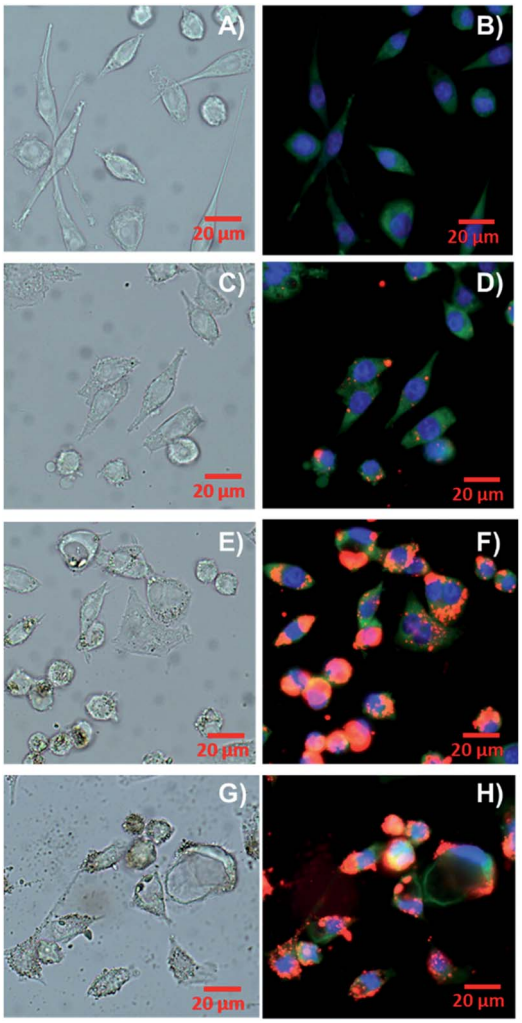

Fig. 4 Bright field (A, C, E and G) and fluorescence (B, D, F and H) microscopy of RAW 264.7 cells exposed to control (A + B), 0.005 mg mL^{-1} (C + D), 0.05 mg mL^{-1} (E + F), and 0.5 mg mL^{-1} PET-RB NPs (G + H). Cell nuclei are blue, PET-RB NPs are red, and cell cytoplasm is green (the images from individual fluorescence channels are shown in ESI 7†).

Open Access Article. Published on 15 December 2020. Downloaded on 2/15/2026 2:38:43 PM.
This article is licensed under a Creative Commons Attribution-NonCommercial 3.0 Unported Licence.

autofluorescence in the green wavelength it was not possible to determine if PET-RB NPs were associated with lysosomes. At 0.05 mg mL^{-1} PET-RB NPs, particles were observed inside phagocytic bodies, but while several cells had formed a tight phagosome around the NPs, vacuoles with large empty spaces surrounding the NPs were observed at the higher concentration. At the highest concentration, phagosomes enlarged and caused elongated, crescent-shaped nuclei in the periphery of the cells. Morphological changes such as blebs were observed at 0.005 mg mL^{-1}, indicating cell membranes delaminate from cortical cytoskeletal structures.[56] These blebs became more numerous at 0.05 mg mL^{-1}, but not at 0.5 mg mL^{-1}. At 0.5 mg mL^{-1}, condensation and increased fluorescence intensity of the nuclei were observed supporting the cytotoxicity data, indicating that a number of cells were not viable at this concentration.

Conclusions

The environmental presence of fragmented plastics, derived from high-commodity polymers, is an emerging concern with unknown consequences for human health. As a crucial high-commodity polymer and contributor of plastic waste, PET has infiltrated drinking water, food, and beverages in the form of small-scale debris (*i.e.*, microplastics), as shown in various reports. Although current reports have focused on micron-scale PET and other plastics, a potential exists for environmental contamination of nanoscale PET, as well.

This manuscript reports the bottom-up synthesis of PET NPs with hydrodynamic diameters below 200 nm. To support studies in cell models, we incorporated the rhodamine B fluorescent tracer into the PET NPs and measured uptake within RAW264.7 macrophages. Our results showed uptake of PET-RB NPs in the macrophages in a dose–response manner. Our findings suggest that a lower concentration of PET NPs (0.0010 mg mL^{-1}) was required to impact the integrity of the cell membrane of macrophages, as compared to concentrations of PET NPs required to alter mitochondrial activity (0.5 mg mL^{-1}). Clear morphological changes occurred at higher concentrations of PET-RB NPs (0.5 mg mL^{-1}), showing enlarged phagosomes that caused elongation of nuclei and likely cell death. Although more studies are required to further elucidate the effects of the NPs in cell models and other biological systems, this study shows that mammalian macrophage cells are affected by PET nanoscale plastics. The generation of well characterized PET NPs will support future studies to assess downstream biological responses.

Conflicts of interest

There are no conflicts to declare.

Acknowledgements

We thank RTI International for support of this work and thank RTI International team members for support to characterize NPs: Brenda Fletcher (FT-IR), Dr Jean Kim (endotoxin testing), Rodney Snyder (UV-Vis), Randy Ruthowske (NMR), Randi Carter (GC/MS), and Sarah Harrison (TEM). FESEM, XPS and Raman work was performed at the Joint School of Nanoscience and Nanoengineering (JSNN), a member of the Southeastern Nanotechnology Infrastructure Corridor (SENIC) and National Nanotechnology Coordinated Infrastructure (NNCI), which is supported by the National Science Foundation (Grant ECCS-1542174). We thank also JSNN team members for their support: Klinton Davis (FESEM, XPS) and Matthew Craps (Raman).

References

1 M. Gilbert, Chapter 1 - Plastics Materials: Introduction and Historical Development, in *Brydson's Plastics Materials*, ed. M. Gilbert, Butterworth-Heinemann, eighth edn, 2017, pp. 1–18.
2 C. M. Rochman, Microplastics research—from sink to source, *Science*, 2018, **360**(6384), 28.
3 C. M. Rochman, The Complex Mixture, Fate and Toxicity of Chemicals Associated with Plastic Debris in the Marine Environment, in *Marine Anthropogenic Litter*, ed. M. Bergmann, L. Gutow and M. Klages, Springer International Publishing, Cham, 2015, pp. 117–140.
4 A. Cózar, F. Echevarría, J. I. González-Gordillo, X. Irigoien, B. Úbeda, S. Hernández-León, Á. T. Palma, S. Navarro, J. García-de-Lomas, A. Ruiz, M. L. Fernández-de-Puelles and C. M. Duarte, Plastic debris in the open ocean, *Proc. Natl. Acad. Sci. U. S. A.*, 2014, **111**(28), 10239.
5 J. A. Ivar do Sul and M. F. Costa, The present and future of microplastic pollution in the marine environment, *Environ. Pollut.*, 2014, **185**, 352–364.
6 M. Eriksen, L. C. M. Lebreton, H. S. Carson, M. Thiel, C. J. Moore, J. C. Borerro, F. Galgani, P. G. Ryan and J. Reisser, Plastic Pollution in the World's Oceans: More than 5 Trillion Plastic Pieces Weighing over 250,000 Tons Afloat at Sea, *PLoS One*, 2014, **9**(12), e111913.
7 A. A. Horton, C. Svendsen, R. J. Williams, D. J. Spurgeon and E. Lahive, Large microplastic particles in sediments of tributaries of the River Thames, UK - Abundance, sources and methods for effective quantification, *Mar. Pollut. Bull.*, 2017, **114**(1), 218–226.
8 R. Geyer, J. R. Jambeck and K. L. Law, Production, use, and fate of all plastics ever made, *Sci. Adv.*, 2017, **3**(7), e1700782.
9 H. C. A. Lim, Chapter 20 - Thermoplastic Polyesters, in *Brydson's Plastics Materials*, ed. M. Gilbert, Butterworth-Heinemann, eighth edn, 2017, pp. 527–543.
10 https://www.plasticsinsight.com/resin-intelligence/resin-prices/polyethylene-terephthalate/.
11 K. Dutt and R. K. Soni, A review on synthesis of value added products from polyethylene terephthalate (PET) waste, *Polym. Sci., Ser. B*, 2013, **55**(7), 430–452.
12 G. P. Karayannidis and D. S. Achilias, Chemical Recycling of Poly(ethylene terephthalate), *Macromol. Mater. Eng.*, 2007, **292**(2), 128–146.
13 B. Singh and N. Sharma, Mechanistic implications of plastic degradation, *Polym. Degrad. Stab.*, 2008, **93**(3), 561–584.

 © 2021 The Author(s). Published by the Royal Society of Chemistry

Open Access Article. Published on 15 December 2020. Downloaded on 2/15/2026 2:38:43 PM.
This article is licensed under a Creative Commons Attribution-NonCommercial 3.0 Unported Licence.

14 M. Day and D. M. Wiles, Photochemical decomposition mechanism of poly(ethylene terephthalate), *J. Polym. Sci., Part B: Polym. Lett.*, 1971, **9**(9), 665–669.
15 M. Day and D. M. Wiles, Photochemical degradation of poly(ethylene terephthalate). II. Effect of wavelength and environment on the decomposition process, *J. Appl. Polym. Sci.*, 1972, **16**(1), 191–202.
16 M. Day and D. M. Wiles, Photochemical degradation of poly(ethylene terephthalate). III. Determination of decomposition products and reaction mechanism, *J. Appl. Polym. Sci.*, 1972, **16**(1), 203–215.
17 A. Launay, F. Thominette and J. Verdu, Hydrolysis of poly(ethylene terephthalate): a kinetic study, *Polym. Degrad. Stab.*, 1994, **46**(3), 319–324.
18 S. Venkatachalam, S. G. Nayak, J. V. Labde, P. R. Gharal, K. Rao and A. K. Kelkar, Degradation and Recyclability of Poly (Ethylene Terephthalate), in *Polyester*, ed. H. E.-D. M. Saleh, IntechOpen, 2012, DOI: 10.5772/48612.
19 B. E. Oßmann, G. Sarau, H. Holtmannspötter, M. Pischetsrieder, S. H. Christiansen and W. Dicke, Small-sized microplastics and pigmented particles in bottled mineral water, *Water Res.*, 2018, **141**, 307–316.
20 M. Pivokonsky, L. Cermakova, K. Novotna, P. Peer, T. Cajthaml and V. Janda, Occurrence of microplastics in raw and treated drinking water, *Sci. Total Environ.*, 2018, **643**, 1644–1651.
21 D. Schymanski, C. Goldbeck, H.-U. Humpf and P. Fürst, Analysis of microplastics in water by micro-Raman spectroscopy: release of plastic particles from different packaging into mineral water, *Water Res.*, 2018, **129**, 154–162.
22 G. Liebezeit and E. Liebezeit, Synthetic particles as contaminants in German beers, *Food Addit. Contam., Part A*, 2014, **31**(9), 1574–1578.
23 A. A. Koelmans, N. H. Mohamed Nor, E. Hermsen, M. Kooi, S. M. Mintenig and J. De France, Microplastics in freshwaters and drinking water: critical review and assessment of data quality, *Water Res.*, 2019, **155**, 410–422.
24 M. E. Iñiguez, J. A. Conesa and A. Fullana, Microplastics in Spanish Table Salt, *Sci. Rep.*, 2017, **7**(1), 8620.
25 M. Fischer, I. Goßmann and B. M. Scholz-Böttcher, Fleur de Sel—An interregional monitor for microplastics mass load and composition in European coastal waters?, *J. Anal. Appl. Pyrolysis*, 2019, **144**, 104711.
26 L. Van Cauwenberghe and C. R. Janssen, Microplastics in bivalves cultured for human consumption, *Environ. Pollut.*, 2014, **193**, 65–70.
27 L. G. A. Barboza, C. Lopes, P. Oliveira, F. Bessa, V. Otero, B. Henriques, J. Raimundo, M. Caetano, C. Vale and L. Guilhermino, Microplastics in wild fish from North East Atlantic Ocean and its potential for causing neurotoxic effects, lipid oxidative damage, and human health risks associated with ingestion exposure, *Sci. Total Environ.*, 2020, **717**, 134625.
28 M. Eriksen, N. Maximenko, M. Thiel, A. Cummins, G. Lattin, S. Wilson, J. Hafner, A. Zellers and S. Rifman, Plastic pollution in the South Pacific subtropical gyre, *Mar. Pollut. Bull.*, 2013, **68**(1), 71–76.
29 X. Guo and J. Wang, The chemical behaviors of microplastics in marine environment: a review, *Mar. Pollut. Bull.*, 2019, **142**, 1–14.
30 M. A. Browne, P. Crump, S. J. Niven, E. Teuten, A. Tonkin, T. Galloway and R. Thompson, Accumulation of Microplastic on Shorelines Worldwide: Sources and Sinks, *Environ. Sci. Technol.*, 2011, **45**(21), 9175–9179.
31 P. J. Kole, A. J. Löhr, F. G. A. J. Van Belleghem and A. M. J. Ragas, Wear and Tear of Tyres: A Stealthy Source of Microplastics in the Environment, *Int. J. Environ. Res. Public Health*, 2017, **14**(10), 1265.
32 A. L. Andrady, Microplastics in the marine environment, *Mar. Pollut. Bull.*, 2011, **62**(8), 1596–1605.
33 N. B. Hartmann, T. Hüffer, R. C. Thompson, M. Hassellöv, A. Verschoor, A. E. Daugaard, S. Rist, T. Karlsson, N. Brennholt, M. Cole, M. P. Herrling, M. C. Hess, N. P. Ivleva, A. L. Lusher and M. Wagner, Are We Speaking the Same Language? Recommendations for a Definition and Categorization Framework for Plastic Debris, *Environ. Sci. Technol.*, 2019, **53**(3), 1039–1047.
34 A. J. Verschoor, *Towards a definition of microplastics: Considerations for the specification of physico-chemical properties*, National Institute for Public Health and the Environment, Bilthoven: RIVM, 2015.
35 C. Arthur, J. Baker and H. Bamford, in *Proceedings of the International Research Workshop on Microplastic Marine Debris*, NOAA Technical Memorandum, NOS-OR&R-30, 2009.
36 H. Bouwmeester, P. C. H. Hollman and R. J. B. Peters, Potential Health Impact of Environmentally Released Micro- and Nanoplastics in the Human Food Production Chain: Experiences from Nanotoxicology, *Environ. Sci. Technol.*, 2015, **49**(15), 8932–8947.
37 A. Nel, T. Xia, L. Mädler and N. Li, Toxic Potential of Materials at the Nanolevel, *Science*, 2006, **311**(5761), 622.
38 A. Nel, T. Xia, H. Meng, X. Wang, S. Lin, Z. Ji and H. Zhang, Nanomaterial Toxicity Testing in the 21st Century: Use of a Predictive Toxicological Approach and High-Throughput Screening, *Acc. Chem. Res.*, 2013, **46**(3), 607–621.
39 J. Jeevanandam, A. Barhoum, Y. S. Chan, A. Dufresne and M. K. Danquah, Review on nanoparticles and nanostructured materials: history, sources, toxicity and regulations, *Beilstein J. Nanotechnol.*, 2018, **9**, 1050–1074.
40 N. P. Mortensen, L. M. Johnson, K. D. Grieger, J. L. Ambroso and T. R. Fennell, Biological interactions between nanomaterials and placental development and function following oral exposure, *Reprod. Toxicol.*, 2019, **90**, 150–165.
41 T. R. Fennell, N. P. Mortensen, S. R. Black, R. W. Snyder, K. E. Levine, E. Poitras, J. M. Harrington, C. J. Wingard, N. A. Holland, W. Pathmasiri and S. C. J. Sumner, Disposition of intravenously or orally administered silver nanoparticles in pregnant rats and the effect on the biochemical profile in urine, *J. Appl. Toxicol.*, 2017, **37**(5), 530–544.

Open Access Article. Published on 15 December 2020. Downloaded on 2/15/2026 2:38:43 PM.
This article is licensed under a Creative Commons Attribution-NonCommercial 3.0 Unported Licence.

42 T. Hüffer, A.-K. Weniger and T. Hofmann, Sorption of organic compounds by aged polystyrene microplastic particles, *Environ. Pollut.*, 2018, **236**, 218–225.
43 T. Xia, M. Kovochich, M. Liong, J. I. Zink and A. E. Nel, Cationic Polystyrene Nanosphere Toxicity Depends on Cell-Specific Endocytic and Mitochondrial Injury Pathways, *ACS Nano*, 2008, **2**(1), 85–96.
44 S. Behzadi, V. Serpooshan, W. Tao, M. A. Hamaly, M. Y. Alkawareek, E. C. Dreaden, D. Brown, A. M. Alkilany, O. C. Farokhzad and M. Mahmoudi, Cellular uptake of nanoparticles: journey inside the cell, *Chem. Soc. Rev.*, 2017, **46**(14), 4218–4244.
45 D. Magrì, P. Sánchez-Moreno, G. Caputo, F. Gatto, M. Veronesi, G. Bardi, T. Catelani, D. Guarnieri, A. Athanassiou, P. P. Pompa and D. Fragouli, Laser Ablation as a Versatile Tool To Mimic Polyethylene Terephthalate Nanoplastic Pollutants: Characterization and Toxicology Assessment, *ACS Nano*, 2018, **12**(8), 7690–7700.
46 F. M. Bauers, R. Thomann and S. Mecking, Submicron Polyethylene Particles from Catalytic Emulsion Polymerization, *J. Am. Chem. Soc.*, 2003, **125**(29), 8838–8840.
47 A. G. Rodríguez-Hernández, J. A. Muñoz-Tabares, J. C. Aguilar-Guzmán and R. Vazquez-Duhalt, A novel and simple method for polyethylene terephthalate (PET) nanoparticle production, *Environ. Sci.: Nano*, 2019, **6**(7), 2031–2036.
48 M. Kokkinopoulou, J. Simon, K. Landfester, V. Mailänder and I. Lieberwirth, Visualization of the protein corona: towards a biomolecular understanding of nanoparticle-cell-interactions, *Nanoscale*, 2017, **9**(25), 8858–8870.
49 P. Eaton, P. Quaresma, C. Soares, C. Neves, M. P. de Almeida, E. Pereira and P. West, A direct comparison of experimental methods to measure dimensions of synthetic nanoparticles, *Ultramicroscopy*, 2017, **182**, 179–190.
50 M. Edge, R. Wiles, N. S. Allen, W. A. McDonald and S. V. Mortlock, Characterisation of the species responsible for yellowing in melt degraded aromatic polyesters—I: Yellowing of poly(ethylene terephthalate), *Polym. Degrad. Stab.*, 1996, **53**(2), 141–151.
51 A. P. d. S. Pereira, M. H. P. d. Silva, É. P. Lima Júnior, A. d. S. Paula and F. J. Tommasini, Processing and Characterization of PET Composites Reinforced With Geopolymer Concrete Waste, *Mater. Res.*, 2017, **20**, 411–420.
52 I. Donelli, G. Freddi, V. A. Nierstrasz and P. Taddei, Surface structure and properties of poly-(ethylene terephthalate) hydrolyzed by alkali and cutinase, *Polym. Degrad. Stab.*, 2010, **95**(9), 1542–1550.
53 R. Dukali, I. Radović, D. Stojanović, D. Sevic, V. Radojevic, D. Jocic and R. Aleksic, Electrospinning of laser dye rhodamine B-doped poly(methyl methacrylate) nanofibers, *J. Serb. Chem. Soc.*, 2014, **79**, 867.
54 M. B. Gorbet and M. V. Sefton, Endotoxin: the uninvited guest, *Biomaterials*, 2005, **26**(34), 6811–6817.
55 Services U. S. D. o. H. a. H., *Guidance for Industry: Pyrogen and Endotoxins Testing: Questions and Answers*, Administration F. a. D., 2012.
56 M. Olson and L. Julian, Apoptotic membrane dynamics in health and disease, *Cell Health Cytoskeleton*, 2015, **7**, 133.

 © 2021 The Author(s). Published by the Royal Society of Chemistry